the pulse intensity is responsible for the optimization results can also be seen from the following argument. In the maximization as well as in the minimization experiment, the increased pulse duration leads to a reduced laser pulse intensity in the time domain as compared with the bandwidth-limited laser pulse. But in one case this reduction leads to a maximization, and in the other case it leads to a minimization, of the desired product branching ratio. It is therefore not possible to obtain the same or similar results by a trivial intensity reduction. Although it is not certain that the algorithm has found the global optimum, significant control between the two reaction channels was achieved, which cannot be obtained by a trivial adjustment of the laser pulse length or the laser pulse intensity.

The results demonstrate automated coherent control of photodissociation reactions with tailored femtosecond laser pulses from a computer-controlled pulse shaper. No information about the sample substance is needed in the optimization procedure, which always started with completely random genetic configurations. By directly optimizing different final product yields of bond-breaking reactions, we achieve a qualitative change from electronic population manipulation toward direct control of different reaction channels. The experiments reported here represent a step toward synthesizing chemical substances with higher efficiencies while at the same time reducing unwanted by-products.

### References and Notes

1. W. S. Warren, H. Rabitz, M. Dahleh, *Science* **259**, 1581 (1993).
2. W. S. Warren, *ibid.* **262**, 1008 (1993); J. Manz and L. Wöste, Eds., *Femtosecond Chemistry* (VCH, Weinheim, Germany, 1995); P. Gaspard and I. Burghardt, Eds., *Chemical Reactions and Their Control on the Femtosecond Time Scale, XXth Solvay Conference on Chemistry* (Wiley, New York, 1997); R. J. Gordon and S. A. Rice, *Annu. Rev. Phys. Chem.* **48**, 601 (1997).
3. R. V. Ambartsumian and V. S. Letokhov, in *Chemical and Biochemical Applications of Lasers*, C. B. Moore, Ed. (Academic Press, New York, 1977), vol. 3, chapter 2; V. S. Letokhov, *Phys. Today* **30**, 23 (May 1977); N. Bloembergen and E. Yablonovitch, *ibid.* **31**, 23 (May 1978); A. H. Zewail, *ibid.* **33**, 27 (November 1980); J. Jortner, R. D. Levine, S. A. Rice, Eds., *Advances in Chemical Physics*, vol. 47, *Photoselective Chemistry* (Wiley, New York, 1981).
4. P. Brumer and M. Shapiro, *Chem. Phys. Lett.* **126**, 541 (1986); M. Shapiro, J. W. Hepburn, P. Brumer, *ibid.* **149**, 451 (1988); P. Brumer and M. Shapiro, *Chem. Phys.* **139**, 221 (1989).
5. C. Chen, Y.-Y. Yin, D. S. Elliott, *Phys. Rev. Lett.* **64**, 507 (1990); S. M. Park, S. P. Lu, R. J. Gordon, *J. Chem. Phys.* **94**, 8622 (1991).
6. D. J. Tannor and S. A. Rice, *J. Chem. Phys.* **83**, 5013 (1985); D. J. Tannor, R. Kosloff, S. A. Rice, *ibid.* **85**, 5805 (1986).
7. T. Baumert, M. Grosser, R. Thalweiser, G. Gerber, *Phys. Rev. Lett.* **67**, 3753 (1991); E. D. Potter, J. L. Herek, S. Pedersen, Q. Liu, A. H. Zewail, *Nature* **355**, 66 (1992); T. Baumert and G. Gerber, *Isr. J. Chem.* **34**, 103 (1994); J. L. Herek, A. Materny, A. H. Zewail, *Chem. Phys. Lett.* **228**, 15 (1994).
8. S. Shi, A. Woody, H. Rabitz, *J. Chem. Phys.* **88**, 6870 (1988).
9. A. P. Peirce, M. A. Dahleh, H. Rabitz, *Phys. Rev. A* **37**, 4950 (1988); R. Kosloff, S. A. Rice, P. Gaspard, S. Tersigni, D. J. Tannor, *Chem. Phys.* **139**, 201 (1989); W. Jakubetz, J. Manz, H.-J. Schreier, *Chem. Phys. Lett.* **165**, 100 (1990).
10. R. S. Judson and H. Rabitz, *Phys. Rev. Lett.* **68**, 1500 (1992).
11. B. Amstrup, G. J. Tóth, G. Szabó, A. Lörincz, *J. Phys. Chem.* **99**, 5206 (1995).
12. B. Amstrup, J. D. Doll, R. A. Sauerbrey, G. Szabó, A. Lörincz, *Phys. Rev. A* **48**, 3830 (1993).
13. T. Baumert, T. Brixner, V. Seyfried, M. Strehle, G. Gerber, *Appl. Phys. B* **65**, 779 (1997).
14. D. Yelin, D. Meshulach, Y. Silberberg, *Opt. Lett.* **22**, 1793 (1997).
15. C. J. Bardeen *et al.*, *Chem. Phys. Lett.* **280**, 151 (1997).
16. R. N. Zare, *Science* **279**, 1875 (1998).
17. A. M. Weiner, D. E. Leaird, J. S. Patel, J. R. Wullert II, *IEEE J. Quantum Electron.* **28**, 908 (1992).
18. O. E. Martínez, *ibid.* **24**, 2530 (1988).
19. B. A. Mamyrin, *Int. J. Mass Spectrom. Ion Processes* **131**, 1 (1994).
20. D. E. Goldberg, *Genetic Algorithms in Search, Optimization, and Machine Learning* (Addison-Wesley, Reading, UK, 1993); H.-P. Schwefel, *Evolution and Optimum Seeking* (Wiley, New York, 1995).
21. I. Wender and P. Pino, Eds., *Organic Synthesis via Metal Carbonyls* (Wiley, New York, 1977), vols. 1 and 2.
22. R. L. Jackson *et al.*, in *Laser Microfabrication*, D. J. Ehrlich and J. Y. Tsao, Eds. (Academic Press, New York, 1989), pp. 385–451.
23. L. Bañares, T. Baumert, M. Bergt, B. Kiefer, G. Gerber, *J. Chem. Phys.* **108**, 5799 (1998).

24. We gratefully acknowledge cooperation with the group of W. Malisch within the Sonderforschungsbereich 347 located at the University of Würzburg. Financial support of the Fonds der chemischen Industrie is also gratefully acknowledged.

8 June 1998; accepted 2 October 1998

---

# The Effect of Alumina on the Electrical Conductivity of Silicate Perovskite

**Yousheng Xu,* Catherine McCammon, Brent T. Poe**

**Measurements of the electrical conductivity of silicate perovskite at 25 gigapascals and 1400° to 1600°C show that the conductivity of (Mg,Fe)$SiO_3$ perovskite containing 2.89 weight percent $Al_2O_3$ is about 3.5 times greater than that of aluminum-free ($Mg_{0.915}Fe_{0.085}$)$SiO_3$ perovskite. The conduction mechanism in perovskite between 1400° and 1600°C is most likely by polarons, because Mössbauer studies show that the aluminum-bearing perovskite has about 3.5 times the amount of $Fe^{3+}$ as the aluminum-free sample. A conductivity-depth profile from 660 to 2900 kilometers based on aluminum-bearing perovskite is consistent with geophysical models.**

The lower mantle consists predominantly of (Mg,Fe)$SiO_3$ perovskite coexisting with about 20% (Mg,Fe)O by volume. Aluminum is a minor element in the lower mantle, and it mainly goes into the perovskite phase (*1*). The partitioning of Fe and Mg between perovskite and magnesiowüstite is strongly coupled to $Al_2O_3$ concentration (*2*), and the proportion of $Fe^{3+}$ in perovskite may increase greatly if perovskite contains a small amount of $Al_2O_3$ (*3*). If the conduction mechanism for perovskite is electron hopping from $Fe^{2+}$ to $Fe^{3+}$ (*4*), the electrical conductivity of perovskite should depend on the concentration of $Fe^{3+}$ and is thus sensitive to substitution of $Al_2O_3$ into perovskite. Here, we evaluate this notion using in situ electrical conductivity measurements of perovskite at lower mantle conditions.

The starting materials for coexperiments were two polycrystalline pyroxene samples with similar Fe/(Fe + Mg) ratios: San Carlos ($Mg_{0.912}Fe_{0.088}$)$SiO_3$ orthopyroxene containing 2.89% $Al_2O_3$ by weight and an Al-free synthetic orthopyroxene, ($Mg_{0.915}Fe_{0.085}$)$SiO_3$. The samples were first transformed to perovskite at 25 GPa and 1600°C in a multianvil apparatus and then prepared as disks for in situ complex impedance spectroscopy in subsequent experiments at 25 GPa and 1400° to 1600°C (*5*).

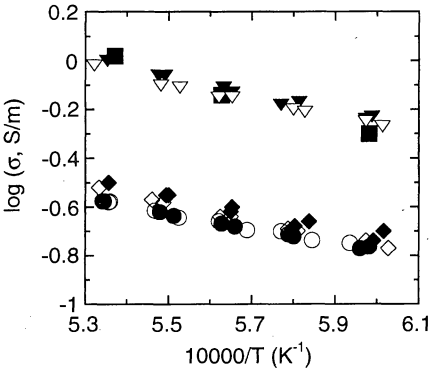

**Fig. 1.** Electrical conductivity of perovskite as a function of reciprocal temperature at 25 GPa. Squares and inverted triangles are for Al-bearing perovskite H826 and H858, respectively, and diamonds and circles are for Al-free perovskite H852 and H862, respectively. Closed symbols refer to the first heating and cooling cycle and open symbols refer to the second heating and cooling cycle.

---

Bayerisches Geoinstitut, Universität Bayreuth, D-95440 Bayreuth, Germany

*To whom correspondence should be addressed. E-mail: yousheng.xu@uni-bayreuth.de

The conductivity measurements were carried out in 10-mm octahedral pressure cells with cubes truncated to 4 mm with a parallel electrode method with a shield connected to ground where sample resistance was determined with impedance spectroscopy (*6*, *7*). The conductivity measurements were likely performed in the presence of a Mo-$MoO_2$ buffer, which maintains an oxygen fugacity close to the iron-wüstite buffer at these conditions (*6–8*).

X-ray diffraction, electron microprobe analysis, and optical microscopic examination before and after conductivity measurements show that there was no evidence of minor phases in the Al-free perovskite and only ~2% majorite and ~3% of a second silicate phase (probably ringwoodite) in the Al-bearing perovskite. The small amounts of these two minor phases have little effect on bulk conductivity because the grains are homogeneously distributed in perovskite and are not interconnected. The geometric distortion of the sample was small and may introduce a maximum uncertainty of 20% in the results (*9*).

Conductivities were fit to the equation

$$\sigma \doteq \sigma_0 e^{-\Delta H/kT} \qquad (1)$$

where $\sigma_0$ is a preexponential factor, $\Delta H$ is activation enthalpy, $k$ is the Boltzmann constant, and $T$ is temperature (Fig. 1).

Results for experiments run in two heating and cooling cycles at 25 GPa and 1400° to 1600°C, as well as results for a repeated run for each perovskite, are identical (*10*). The results show that the activation energy of 0.70 eV for conduction in perovskite containing 2.89% $Al_2O_3$ by weight is close to the value of 0.62 eV for conduction in Al-free perovskite (Fig. 1 and Table 1). However, the electrical conductivity of the Al-bearing perovskite is about 3.5 times that of the Al-free perovskite.

The relative amount of $Fe^{3+}$ in these perovskites was determined with Mössbauer spectroscopy (*11*). The results show that $Fe^{3+}/\Sigma Fe$ in the Al-bearing perovskite (~42 ± 5%) is also about 3.5 times greater than that in the Al-free perovskite (~12 ± 3%) synthesized at 25 GPa and 1600°C (Table 2). These data are similar to those of McCammon (*3*) for similar compositions. The similarity between the effects of $Al_2O_3$ on the electrical conductivity and the amount of $Fe^{3+}$ in perovskite (the factor of 3.5) (Table 2) indicates that electrical conductivity of perovskite is proportional to the amount of $Fe^{3+}$. This observation suggests the hypothesis that the conduction mechanism in perovskite between 1400° and 1600°C is most likely by polarons, for example, by electron hopping ($Fe^{2+} \rightarrow Fe^{3+} + e^-$).

In comparison with previous data (Fig. 2), the absolute values are around the same as those of Katsura *et al.* (*12*), but the activation energies of 0.62 to 0.70 eV for conduction in perovskite are lower than the value of 0.92 eV obtained by Katsura *et al.* (*12*). A calculation (*13*) shows that the higher activation energy obtained by Katsura *et al.* (*12*) could be caused by increasing leakage current through their $Al_2O_3$ container. This difference between our results and the value of ~0.33 eV determined for perovskite in diamond anvil studies at lower temperatures (25° to 400°C) (Fig. 2) (*4*) likely results from nonequilibrium (quenched) conditions at low temperature (*14*). Activation energies and zero pressure conductivities in this study are much higher than those reported by Li and Jeanloz (*15*) up to ~3250°C (Fig. 2), probably because of the difficulties of controlling, for example, temperature gradients and oxygen fugacity in a laser-heated diamond anvil cell.

Perovskite is likely to govern the bulk electrical conductivity of the lower mantle. In peridotitic mantle, the perovskite phase should contain 4 to 5% $Al_2O_3$ by weight (*16*). A conductivity-depth profile for the lower mantle can be constructed from Eq. 1 with the Al-bearing perovskite parameters (run H858) from Table 1 (Fig. 3). To simplify this laboratory-based conductivity model, we did not consider the pressure effects for perovskite, effects of oxygen fugacity, possible OH in the minerals, the presence of other mineral phases, or texture (*17*). The temperature gradient for the lower mantle was taken from Boehler (*18*).

Our results show that electrical conductivity reaches a value of about 1 S/m at the top of the lower mantle, in agreement with geomagnetic determinations (*19–22*) (Fig. 3). The laboratory-based model for the lower mantle is consis-

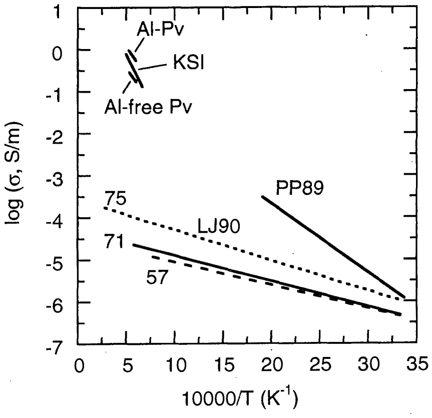

**Fig. 2.** Electrical conductivity of perovskite as a function of reciprocal temperature compared with previous results. KSI (*12*) is $(Mg_{0.93}Fe_{0.07})SiO_3$ Al-free perovskite at 23 GPa, PP89 (*24*) is $(Mg_{0.915}Fe_{0.085})SiO_3$ Al-bearing perovskite at 40 GPa, and LJ90 (*15*) is $(Mg_{0.88}Fe_{0.12})SiO_3$ perovskite at the three pressures indicated.

**Table 1.** Activation enthalpies and preexponential terms from fitting Eq. 1 to the experimental data at 25 GPa and 1400° to 1600°C. Pv, perovskite.

| Sample | Run | $\log(\sigma_0)$ | $\sigma_0$ (S/m) | $\Delta H$ (eV) |
|---|---|---|---|---|
| Al-bearing Pv | H826* | 2.80 ± 0.27 | 631 | 1.03 ± 0.09 |
| Al-bearing Pv | H858 | 1.87 ± 0.11 | 74 | 0.70 ± 0.04 |
| Al-free Pv | H852 | 1.31 ± 0.13 | 20 | 0.68 ± 0.05 |
| Al-free Pv | H862 | 1.06 ± 0.04 | 11 | 0.61 ± 0.01 |
| Al-free Pv | Average† | 1.12 ± 0.12 | 11 | 0.62 ± 0.04 |

*Only three data points were obtained, and the uncertainty of the fitting parameters is potentially large. Therefore, the conductivity model of the lower mantle was based on the fitting parameters of H858 only. †The average parameters of Al-free perovskite were obtained by fitting all data of H852 and H862.

**Table 2.** Electrical conductivity and the amount of $Fe^{3+}$ in Al-bearing and Al-free perovskite (Pv) at 25 GPa and ~1600°C.

| | Al-bearing Pv | Al-free Pv | Al-bearing Pv/Al-free Pv | Reference |
|---|---|---|---|---|
| σ (S/m) | 0.97 | 0.28 | ~3.5 | This work |
| $Fe^{3+}/\Sigma Fe$ | 42 ± 5% | 12 ± 3% | 3.5 | This work |
| $Fe^{3+}/\Sigma Fe$ | 50 ± 5% | 16 ± 3% | ~3.1 | (*3*) |

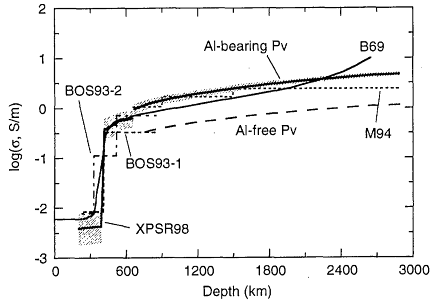

**Fig. 3.** Conductivity models for the lower mantle calculated from the data of Al-bearing perovskite (thick line) and Al-free perovskite (long dashed line) together with the upper mantle laboratory-based curve XPSR98 (thick line) (*7*). Shaded areas illustrate the effect on the model of a ±100°C temperature variation. Geophysical models are shown as B69 (thin line) (*19*), M94 (dotted line) (*20*), BOS93-1 (dashed line) (*21*), and BOS93-2 (dot-dash line) (*21*).

tent with geophysical models, for example, B69 (*19*) and M94 (*20*). In comparing our laboratory-based lower mantle model with upper mantle model XPSR98 (*7*), we found a conductivity jump of two orders of magnitude at the 410-km discontinuity and a minor conductivity increase at 660-km depth where ringwoodite disproportionates to perovskite + magnesiowüstite.

According to the conductivity variation for a temperature variation of ±100°C, our results do not favor temperature increasing along the $(Mg_{0.88}Fe_{0.12})SiO_3$ perovskite 2000°C adiabat from 2300°C at 660-km depth (*23*) if the effects of $Al_2O_3$ on the conductivity of silicate perovskite are considered.

### References and Notes

1. T. Irifune and A. E. Ringwood, in *High-Pressure Research in Mineral Physics*, vol. 39 of *Geophysical Monograph Series* (American Geophysical Union, Washington, DC, 1987), pp. 231–242; T. Irifune, *Nature* **370**, 131 (1994).
2. B. J. Wood and D. C. Rubie, *Science* **273**, 1522 (1996).
3. C. McCammon, *Nature* **387**, 694 (1997).
4. Negative activation volumes of 0.26 ± 0.03 $cm^3$ $mol^{-1}$ for perovskite and 0.1 to 0.2 $cm^3$ $mol^{-1}$ for perovskite-magnesiowüstite assemblages are consistent with the hopping conduction mechanism [(*24*); T. J. Shankland, J. Peyronneau, J.-P. Poirier, *Nature* **366**, 453 (1993); J. P. Poirier, A. Goddat, J. Peyronneau, *Philos. Trans. R. Soc. London Ser. A* **354**, 1361 (1996)].
5. After the sample was placed inside the octahedral pressure medium, the entire cell assembly was dried overnight at 70°C in a vacuum furnace.
6. Y. Xu, B. T. Poe, D. C. Rubie, in *The Review of High Pressure Science and Technology, Proceedings of JOINT AIRAPT-16 & HPCJ-38*, M. Nakahara, Ed. (Japan Society of High-Pressure Science and Technology, Kyoto, Japan, 1998), vol. 7, pp. 1526–1528.
7. Y. Xu, B. T. Poe, T. J. Shankland, D. C. Rubie, *Science* **280**, 1415 (1998) (Model XPSR98).
8. MgO rings are also in contact with the sample but have no effect on oxygen fugacity.
9. Conductivity $\sigma = 1/RQ$, where $R$ is the resistance of sample and $Q = A/l$ is the geometric factor of the recovered sample ($A = \pi r^2$ is the area of the electrodes and $l$ is the length of the sample). The maximum error of the sample's geometry is 20% according to microscopic examination.
10. The conductivities in results from duplicate experiments differ by less than 0.07 logarithmic units, where the difference is likely due to uncertainty in sample geometry (a maximum uncertainty in geometry of 20% gives a difference of 0.08 logarithmic units in conductivity).
11. Samples identical to those used for conductivity measurements were synthesized at the same conditions and examined with the Mössbauer milliprobe according to the procedure described previously [C. A. McCammon, M. Hutchison, J. Harris, *Science* **278**, 434 (1997)]. Mössbauer spectra of the samples show the presence of $Fe^{2+}$ and $Fe^{3+}$ and rapid electron transfer between $Fe^{2+}$ and $Fe^{3+}$. The relative amount of $Fe^{3+}$ can be determined from the relative areas corrected for differences in recoil-free fraction [C. A. McCammon, *Phys. Chem. Miner.* **25**, 292 (1998)].
12. T. Katsura, K. Sato, E. Ito, *Nature* **395**, 493 (1998) (Model KSI).
13. Katsura *et al.* (*12*) used an electrode with an area larger than the sample area, and the geometric factor of the $Al_2O_3$ container is about three times greater than that of the sample. According to previous results for $Al_2O_3$ [A. Duba, in *High-Pressure Researches in Geoscience*, W. Schreyer, Ed. (Schweizerbart'sche Verlagsbuchhandlung, Stuttgart, Germany, 1982), pp. 375–381], the conductivity of $Al_2O_3$ is only ~0.5 logarithmic units lower than that of the sample at 1600°C. This result implies that leakage current through the $Al_2O_3$ container could be equal to that through the sample at 1600°C. The activation energy should increase with temperature, because the activation energy of ~2.5 eV for $Al_2O_3$ is much higher than that of perovskite.
14. The quenched phase should maintain the proportion of $Fe^{3+}$ at high temperature and cannot reach equilibrium at low temperature in a short time.
15. X. Li and R. Jeanloz, *J. Geophys. Res.* **95**, 5067 (1990).
16. A. E. Ringwood, *Composition and Petrology of the Earth's Mantle* (McGraw-Hill, New York, 1975).
17. The effect of pressure on conductivity is weak, and the activation volume should be small (*4*). The electrical conductivity of perovskite is sensitive to the amount of $Fe^{3+}$ coupled with $Al_2O_3$, and so the effect of oxygen fugacity on Al-bearing perovskite is small. The effect of OH on the conductivity of silicate perovskite is still unknown. The effect of texture at high pressure is small if different minerals are homogeneously distributed and there is no partial melt present.
18. R. Boehler, *Annu. Rev. Earth Planet. Sci.* **24**, 15 (1996).
19. R. J. Banks, *Geophys. J. R. Astron. Soc.* **17**, 457 (1969) (model B69).
20. K. G. McLeod, *J. Geophys. Res.* **99**, 13577 (1994) (model M94).
21. K. Bahr, N. Olsen, T. J. Shankland, *Geophys. Res. Lett.* **20**, 2937 (1993) (models BOS93-1 and BOS93-2).
22. H. F. Petersons and S. Constable, *ibid.* **23**, 1461 (1996).
23. I. Jackson, *Geophys. J. Int.* **134**, 291 (1998).
24. J. Peyronneau and J. P. Poirier, *Nature* **342**, 537 (1989) (model PP89).
25. We thank T. J. Shankland, A. G. Duba, and D. C. Rubie for discussions and suggestions and H. Fischer, K. Klasinski, D. Krausse, H. Küfner, and H. Schulze for technical assistance. D. C. Rubie and S. Karato donated the San Carlos orthopyroxene.

22 July 1998; accepted 30 September 1998

# Seismic Evidence for an Inner Core Transition Zone

**Xiaodong Song and Don V. Helmberger**

**Seismic waves that traverse Earth's inner core along north-south paths produce unusually broad pulse shapes at long periods (compared with waves along east-west paths) and reflections from below the inner core boundary at short periods. The observations provide compelling evidence for a seismic velocity discontinuity along north-south paths about 200 kilometers below the inner core boundary separating an isotropic upper inner core from an anisotropic lower inner core. The triplication associated with such a structure might be responsible for reported waveform complexity of short-period inner core arrivals along north-south paths and, if the depth of the boundary is laterally variable, their large travel-time variation.**

Earth's core consists of a solid inner core with a radius of 1220 km surrounded by a liquid iron-rich outer core with a radius of 3480 km. The inner core was formed by the freezing of the liquid outer core as the Earth's interior loses its primordial heat (*1*). It is thought that the slow growth of the inner core provides a source of energy to drive the geodynamo in the fluid outer core, which generates the Earth's magnetic field (*2*). Sixty years after the inner core was discovered in 1936 (*3*), seismic observations revealed that it was rotating relative to the mantle at about 1° per year (*4*). The inner core rotation is driven by magnetic coupling between the electrically conductive inner core and the geomagnetic field (*5*). Subsequent estimates of the rotation vary by one order of magnitude, from 3° per year (*6*) to 0.2° to 0.3° per year (*7*), depending on the measurements of time-dependent signals and the models of inner core anisotropy used to infer the rotation.

The hypothesis that the inner core is anisotropic was first proposed in 1986 (*8*) and the presence of significant anisotropy in the inner core is now well established (*9*). On average, the wave velocity is about 3% faster along north-south (NS) ray paths through the inner core than along east-west (EW) ray paths (*10*). However, the detailed structure of the inner core anisotropy appears to be complex with significant lateral and depth variations (*11–14*). Although anisotropy occurs throughout the bulk of the inner core (*15*), the upper part of the inner core has weak to negligible anisotropy (*11, 12*). In addition, seismograms produced by NS paths show inner core arrivals with smaller amplitudes (*16*) and more complex waveforms (*17*) at short periods. Here we present evidence for a transitional structure of a mostly isotropic upper inner core (UIC) surrounding an anisotropic lower inner core (LIC) (Fig. 1A). We show that the triplication (Fig. 1B) associated with the rapid increase of velocity at such a transition along NS paths provides a consistent explanation for the anomalously broad waveforms of PKP-DF phases (compared with PKP-BC or PKP-AB phases) on long-period and broadband seismograms (dominant period about 10 s) and reflections from within the inner core on short-period seismograms (period about 1 s). The PKP-DF (or simply DF) ray goes through the inner core, whereas the PKP-

---

X. D. Song, Lamont-Doherty Earth Observatory, Palisades, NY 10964, and Department of Earth and Environmental Sciences, Columbia University, New York, NY 10027, USA. D. V. Helmberger, Seismological Laboratory, California Institute of Technology, Pasadena, CA 91125, USA.